Research in Astronomy and Astrophysics, 25:025021 (10pp), 2025 February
https://doi.org/10.1088/1674-4527/adb139
CSTR: 32081.14.RAA.adb139

Constraints on Baryon Density from the Effective Optical Depth of High-redshift Quasars

Wen-Fei Liu[1,5], Yuan-Bo Xie[2,3,5], Zhi-E Liu[1], Jin Qin[3], Kang Jiao[3], Dong-Yao Zhao[4], and Tong-Jie Zhang (张同杰)[2,3]
[1] College of Physics and Electronic Engineering, Qilu Normal University, Jinan 250200, China
[2] Institute for Frontiers in Astronomy and Astrophysics, Beijing Normal University, Beijing 102206, China; tjzhang@bnu.edu.cn
[3] School of Physics and Astronomy, Beijing Normal University, Beijing 100875, China
[4] Beijing Planetarium, Beijing Academy of Science and Technology, Beijing 100044, China
Received 2024 November 18; revised 2025 January 19; accepted 2025 January 29; published 2025 February 21

Abstract

We present constraints on the baryonic matter density parameter, Ω_b, within the framework of the ΛCDM model. Our analysis utilizes observational data on the effective optical depth from high-redshift quasars. To parameterize the photoionization rate Γ_{-12}, we employ a Bézier polynomial. Additionally, we approximate the Hubble parameter at high redshifts as $H(z) \approx 100h\Omega_m^{1/2}(1+z)^{3/2}\,\mathrm{km\,s^{-1}\,Mpc^{-1}}$. Confidence regions are obtained with $h = 0.701 \pm 0.013$ and $\Omega_m = 0.315$, optimized by the Planck mission. The best-fit values are $\Omega_b = 0.043^{+0.005}_{-0.006}$ and $\Omega_b = 0.045^{+0.004}_{-0.006}$, corresponding to an old data set and a new data set, respectively. We test the non-parametric form of Γ_{-12}, obtaining $\Omega_b = 0.048^{+0.001}_{-0.003}$. These results are consistent with the findings of Planck at the 1σ confidence level. Our findings underscore the effectiveness of quasar data sets in constraining Ω_b, eliminating the need for independent photoionization rate data. This approach provides detailed cosmic information about baryon density and the photoionization history of the intergalactic medium.

Key words: cosmology: observations – (cosmology:) cosmological parameters – cosmology: theory

1. Introduction

Quasars are one of the most distant celestial objects that can be observed as luminous sources, often at very high redshifts, with some even approaching the epoch of reionization. This epoch occurred when the first generation of stars and quasars ionized the neutral intergalactic medium (IGM) and ended the cosmic "dark ages" (Holt & Smith 1999). The growing number of observations of high-redshift quasars has provided valuable measurements and made them an effective probe for studying the early universe. Keck and VLT spectroscopy of high-redshift quasars (Becker et al. 2001; Pentericci et al. 2002) have shown the first observation of a complete Gunn–Peterson trough in the spectrum of the $z = 6.28$ quasar SDSS 1030+0524. Becker et al. (2015) have discovered an exceptionally long and dark Lyα trough that extends to high redshifts. This trough represents the longest one found to date below a redshift of 6. Djorgovski et al. (2001) observed a particularly dark region of length approximately 5 Mpc at $z \approx 5.4$ along the line of sight to the $z \approx 5.8$ quasar SDSS 1044–0125. Observations of high-redshift quasars by Fan et al. (2001), Becker et al. (2001), and Pentericci et al. (2002) have shown that the Lyα absorption due to neutral hydrogen in the IGM increases dramatically toward high redshifts.

One of the primary goals of cosmology is to constrain cosmological parameters using various observational quantities that depend on redshift. In this paper, we utilize measurements of the effective optical depth obtained from spectroscopic observations of high-redshift quasars, spanning a redshift range of $z = 4.8$–6.2, to constrain the baryon density parameter, Ω_b. Some of these data sets have previously been employed to investigate the evolution of the ionizing background and the epoch of reionization (Fan et al. 2002, 2006). However, this study represents the first application of these data sets to constrain Ω_b, which is a crucial cosmological parameter commonly determined through the Cosmic Microwave Background (CMB) or the Baryon Acoustic Oscillation (BAO) measurements from galaxy clustering. While these traditional methods are applicable at very high redshifts and relatively low redshift epochs, respectively, our work provides an important complement by utilizing high-redshift quasars to derive constraints on Ω_b within the redshift range between the CMB and galaxies.

In Section 2, we present the observational data. The derivations of the effective optical depth and the constraint methods are introduced in Section 3. Finally, we will discuss and conclude in Section 4.

[5] These authors contributed equally to this work.

2. Observational Data

In this work, we selected the data of effective optical depth for Lyα from Fan et al. (2006) and the up-to-date sample from Bosman et al. (2022) to process cosmological constraints.

For all the spectra in the work of Fan et al. (2006), 12 of the spectra were obtained using the Keck ESI instrument, while the remaining spectra were observed using the MMT Red Channel and Kitt Peak 4 m MARS spectrographs. The data used in this study have a spectral resolution of approximately $R \sim 3000$–6000, which depends on the seeing conditions. They binned all the Keck ESI spectra to a resolution of $R = 2600$. Although the signal-to-noise ratios (S/Ns) of these spectra vary by a factor of approximately 7, they have obtained sufficiently long observations for all quasars at redshifts greater than 6.1 to ensure accurate measurement of complete Gunn–Peterson troughs. The nonuniform S/N among the lower redshift quasars does not significantly affect the analysis. In fact, uncertainties in the average transmission are primarily influenced by large sample variance (Fan et al. 2006).

The data set used in the study by Bosman et al. (2022) includes 30 quasar spectra at $z \gtrsim 5.8$ from the XQR-30 program (1103.A-0817(A)), 26 archival spectra obtained with the X-Shooter spectra of equal SNR > 10 per 10 km s^{-1} pixel, and 16 archival spectra of quasars with $\gtrsim$5.7 obtained with the ESI instrument on the Keck Telescope. All XQR-30 spectra have signal-to-noise ratios (SNRs) greater than 20 per 10 km s^{-1} pixel within the wavelength range of 1165 Å–1170 Å. The X-Shooter instrument provides a resolution of approximately 34 km s^{-1} in the visible range (5500 Å–10200 Å) and approximately 37 km s^{-1} in the infrared range (10200 Å–24800 Å). However, due to better-than-average seeing conditions during observations, the effective resolution is slightly higher. On the other hand, the ESI instrument has a lower spectral resolution of approximately 60 km s^{-1} and its wavelength coverage is limited to the optical range up to $\lambda < 10500$ Å. Figure 1 illustrates the distribution of SNRs for quasars obtained from the XQR-30, X-Shooter, and ESI data sets. The figure clearly demonstrates that, in general, the XQR-30 data set exhibits higher SNR values. All the quasar samples were divided into 14 bins, and the mean Lyα transmission was obtained for each bin.

In this study, we utilize the data from both Fan et al. (2006) and the data set provided by Bosman et al. (2022) to constrain the value of Ω_b. Our analysis yields similar results that are in agreement with the findings of Planck Collaboration et al. (2020) within the 1σ confidence region.

3. Methodology

The effective optical depth is derived with the consideration that the IGM is inhomogeneous. This assumption is reasonable because the actual distribution of the IGM in the universe is complex and inhomogeneous, and therefore would necessarily affect the observations. Additionally, another consideration in the derivation of the theoretical effective optical depth is the approximation of the Hubble parameter at high redshifts. When $z \gg 1$, the Hubble parameter $H(z)$ can be approximated as $H(z) \approx 100h\Omega_m^{1/2}(1+z)^{3/2}\,\mathrm{km\,s^{-1}\,Mpc^{-1}}$. This approximation is advantageous because the observational data are all from quasars at very high redshifts ($z = 4.8 \sim 6.2$), some of which even approach the reionization epoch. We will provide detailed derivations for the effective optical depth below.

3.1. Effective Optical Depth for Lyα

Assuming an approximate thermal equilibrium between photoionization heating by the UV background and adiabatic cooling due to Hubble expansion (Hernquist et al. 1996; Hui & Gnedin 1997), the optical depth for Lyα and Lyman-β absorption lines, also known as the Gunn–Peterson optical depth, depends on the local density of the IGM. Therefore, the non-uniformity of the IGM must be taken into account. The fractional density of the IGM is defined as $\Delta \equiv \rho/\langle\rho\rangle \equiv \delta + 1$ (where δ, the density contrast, is the departure of the local density from the mean density, in units of the mean density). For a region of IGM with density Δ, the effective optical depth can be written as (Fan et al. 2002):

$$\tau(\Delta) \propto \frac{(1+z)^6(\Omega_b h^2)^2\alpha(T)}{\Gamma(z)H(z)}\Delta^2, \tag{1}$$

where Ω_b is the baryon density, $\Gamma(z)$ is the photoionization rate, and $\alpha(T)$ is the recombination coefficient at temperature T (Abel et al. 1997), $\alpha(T) = 4.2 \times 10^{-13}(T/10^4\mathrm{K})^{-0.7}\mathrm{cm^3s^{-1}}$.

The dependence on Δ^2 comes from $\tau \propto n_{\mathrm{H\,I}}$ (Gunn & Peterson 1965), which is proportional to n_{H}^2 (Hernquist et al. 1996), and proportional to Δ^2 for a highly ionized IGM (Fan et al. 2002). The temperature of the IGM is determined by photoionization-recombination equilibrium, which leads to a power-law relation between temperature and density in the form of $T = T_0\Delta^{\gamma-1}$, with $T_0 \sim 1$–2×10^4 K, and γ ranges from -1 to 0 (Hui & Gnedin 1997).

The optical depth for Lyα can be expressed as

$$\tau_\alpha(\Delta) = \tau_0\frac{(1+z)^6}{\Gamma_{-12}(z)}\frac{(\Omega_b h^2)^2}{H(z)}\Delta^2\left(\frac{2}{T(z)}\right)^{0.7}, \tag{2}$$

where $\Gamma_{-12}(z)$ is the photoionization rate in units of $10^{-12}\,\mathrm{s^{-1}}$, whose data matching the redshifts of samplers can be obtained from (Fan et al. 2002, 2006). The numerical constant τ_0 is determined below. $T(z)$ is the temperature in units of 10^4 K, which will be discussed in Section 3.3.

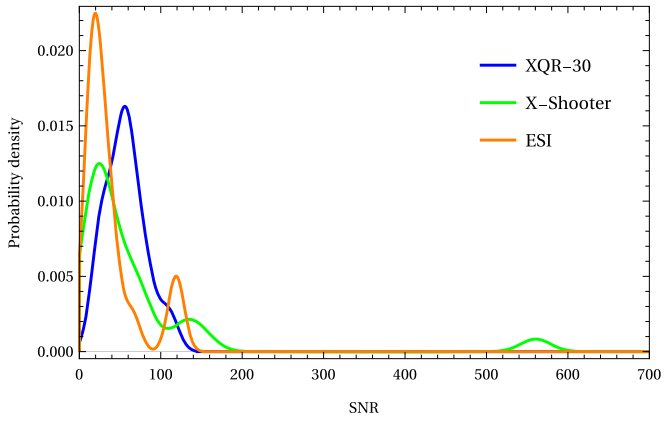

Figure 1. The probability distribution functions of SNR for three different data sets used to construct Bosman et al. (2022) quasar data: XQR-30 (blue), X-Shooter (green), and ESI (orange). It is observed that the SNR distribution for most of the data lies between 10 and 100.

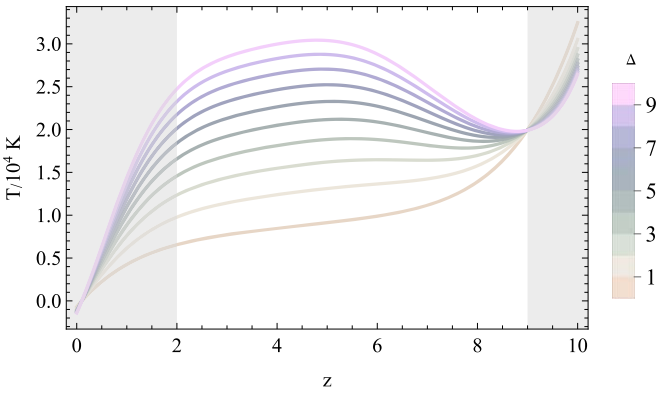

Figure 2. The thermal history, T, with respect to different density Δ, ranges from 1 to 10. The gray areas represent the regions where $z < 2$ and $z > 9$, with no T_0 provided in McQuinn & Upton Sanderbeck (2015); therefore, T may not be reliable in those regions. However, the central region has already covered the redshift range of the data used in this paper. We can observe that when the density is low, the temperature increases monotonically with redshift. However, when the density is high, the temperature approximately reaches a maximum at $z = 5$, and then decreases.

At high redshift $H(z) \approx 100h\Omega_m^{1/2}(1+z)^{3/2}\,\mathrm{km\,s^{-1}\,Mpc^{-1}}$, and the Equation (2) can be rewritten as

$$\tau_\alpha(\Delta) = \tau_1 \frac{(1+z)^{4.5}}{\Gamma_{-12}(z)} \frac{\Omega_b^2}{\Omega_m^{0.5}} h^3 \Delta^2 \left(\frac{2}{T(z)}\right)^{0.7}, \tag{3}$$

where numerical constant $\tau_1 = \tau_0/(3.24 \times 10^{-18})$ (in CGS unit system). We follow McDonald & Miralda-Escudé (2001) and set $\tau_1 = 0.664$, corresponding to $\tau_0 = 2.15 \times 10^{-18}$.

Equation (3) is appropriate for all Lyman series lines, with different values of the proportionality constant (Fan et al. 2006).

The observed transmitted flux ratio $\mathscr{T}$ is averaged over the entire IGM density distribution (Fan et al. 2002)

$$\mathscr{T} = \langle e^{-\tau} \rangle = \int_0^\infty e^{-\tau(\Delta)} p(\Delta) d(\Delta), \tag{4}$$

This equation assumes that the universe is fully ionized. However, several recent studies, for example, Kulkarni et al. (2019), have pointed out that this assumption may not hold true at $z > 5.5$. If the findings of Kulkarni et al. (2019) are accurate, the optical depth will be larger. In order to balance Equation (3), a larger value of Ω_b is required. While we recognize that the assumption of full ionization may not be entirely valid in the redshift range $z = 4.8$–6.2, the IGM is predominantly ionized in this range, meaning that the assumption of full ionization remains approximately valid. Furthermore, the impact on the constraints of Ω_b falls within the acceptable error margins of the parameter limits. To simplify the analysis and maintain consistency with previous studies, we continue to assume a fully ionized universe. It is important to note that our analysis is based on observational data, which generally support the assumption of full ionization in this redshift range, as demonstrated by Fan et al. (2002, 2006). However, future research may benefit from incorporating models with partial ionization, particularly at higher redshifts.

The distribution function of the IGM density, denoted as $p(\Delta)$, is a function of the volume-weighted density distribution (Miralda-Escudé et al. 2000).

$$p(\Delta) = A \exp\left[-\frac{(\Delta^{-2/3} - C_0)^2}{2(2\delta_0/3)^2}\right] \Delta^{-\beta}, \tag{5}$$

The parameter $\delta_0 = 7.61/(1+z)$, where z is the redshift, and the constants β, C_0, and A are numerical values listed in Table 1 of Miralda-Escudé et al. (2000) for various redshifts. These constants are obtained from numerical simulations, which align well with the observational results of the Lya forest transmitted flux (Rauch et al. 1997; Miralda-Escudé et al. 2000).

The definition of effective optical depth is

$$\tau_{\mathrm{GP}}^{\mathrm{eff}} \equiv -\ln(\mathscr{T}), \tag{6}$$

Combining Equations (3), (4), (5) and (6), one can get the final equation for calculating the Lyα theoretical effective optical depth for inhomogeneous IGM with the high-redshift approximation of Hubble parameter.

3.2. Parameterization of the Photoionization Rate Γ_{-12}

In this work, we employ a Bézier fit to describe the evolution of Γ_{-12} with redshift. The parameterization is given by

$$\Gamma_{-12}(z) = \sum_{d=0}^{n} a_d \frac{n!(z/z_m)^d}{d!(n-d)!} \left(1 - \frac{z}{z_{\mathrm{m}}}\right)^{n-d} \tag{7}$$

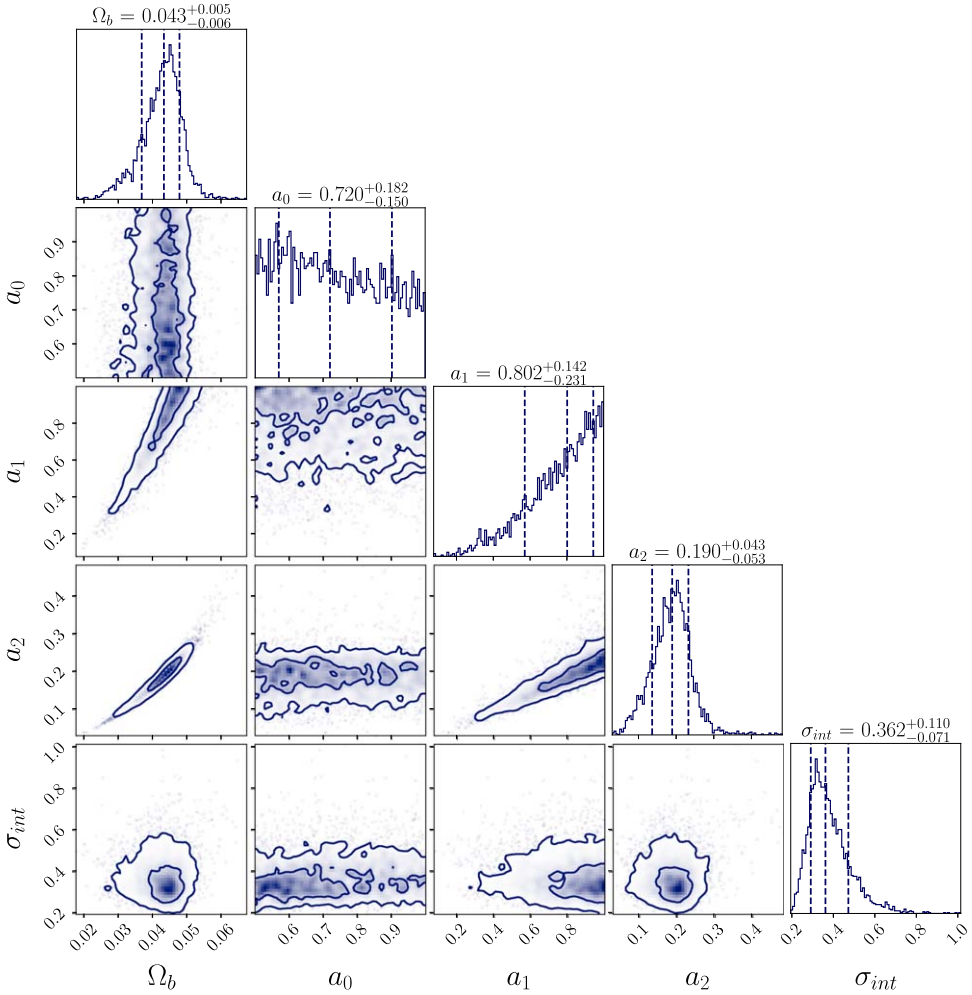

Figure 3. The 1D and 2D contours representing the 1σ and 2σ confidence regions for Fan et al. (2006) Lyα data. It can be seen that although a_0 and a_1 cannot be well constrained, a_2, especially the most important parameter, the baryon density, has been well constrained. The value of the baryon density is consistent with the results of Planck within a 1σ confidence interval.

where z_m is the maximum redshift in the quasar data, and a_d are the coefficients. This method, first introduced by (Amati et al. 2019), has been previously used to reconstruct Hubble data. We set $n = 2$ to balance the trade-off between the flexibility of the parameterization curve, determined by the number of coefficients a_d, and the precision of the fitting results, which is limited by the number of available data points. This parameterization takes the advantage of the flexibility of Bézier curves compared with other curves like polynomials. The flexibility of Bézier is more advantageous for parametric constraints than other curves, such as polynomials.

3.3. Thermal History Parameters

We refer to Figure 2 in McQuinn & Upton Sanderbeck (2015) to establish a reasonable form for $T(z) = T_0(z)\Delta^{\gamma(z)-1}$. The curve depicted in Figure 2 of McQuinn & Upton Sanderbeck (2015) can be well approximated by the following two quintic polynomials.

$$\begin{aligned} T_0(z) &= 0.000276332z^5 - 0.0059786z^4 + 0.0541698z^3 \\ &\quad - 0.257399z^2 + 0.703909z - 0.0692726 \\ \gamma(z) &= 0.000190549z^5 - 0.00480521z^4 + 0.0436158z^3 \\ &\quad - 0.187106z^2 + 0.369498z + 1.308008 \end{aligned} \tag{8}$$

Figure 2 displays the thermal history for different densities ranging from 1 to 10. It is evident that within our region of interest $z \sim (4.8–6.2)$, the form of $T(z)$ will have a significant impact on the optical depth $\tau_\alpha(\Delta)$.

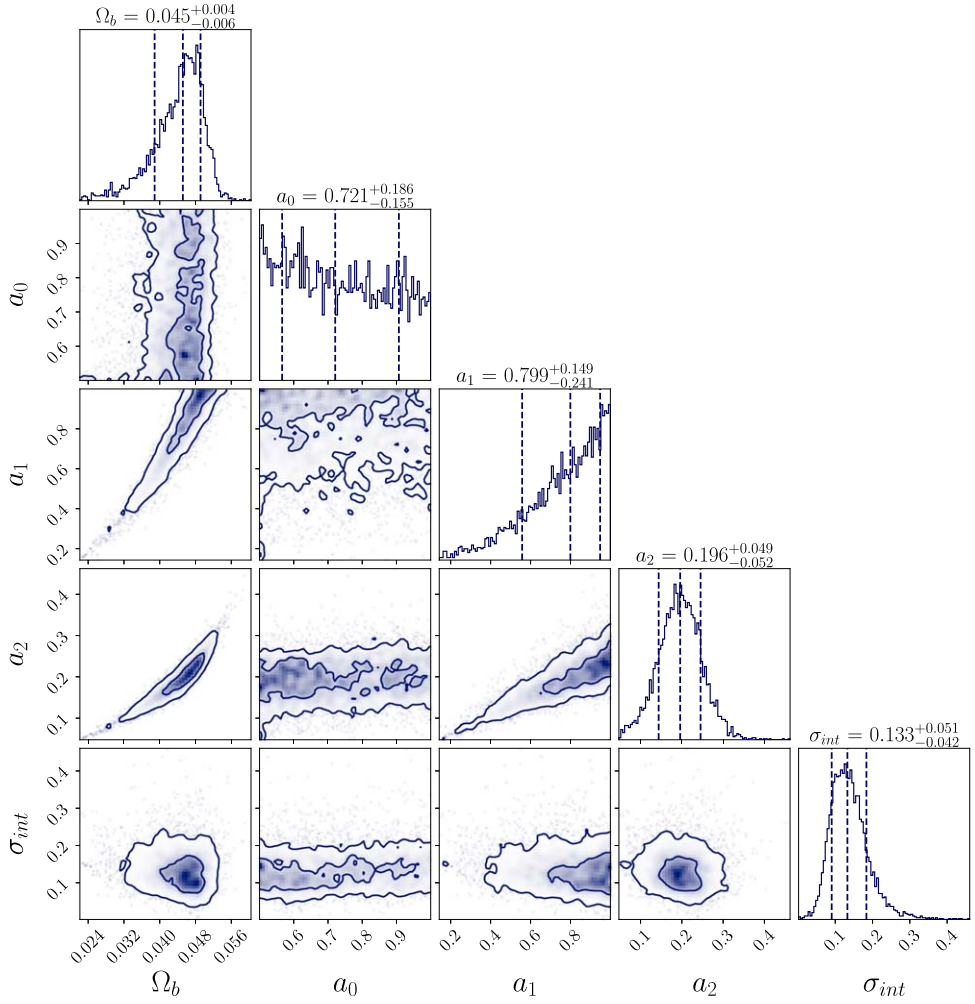

Figure 4. The 1D and 2D contours representing the 1σ and 2σ confidence regions for Bosman et al. (2022) Lyα data. Similar to the results of Figure 3, a_0 and a_1 are not well constrained, but a_2 and the baryon density, Ω_b, are better constrained, and the value of Ω_b is consistent with the Planck results.

3.4. Fitting Methods

Considering that the data are independently and identically distributed as Gaussian, we have a likelihood form as follows

$$\mathscr{L} = \prod_{i=1}^{n} \frac{1}{\sqrt{2\pi\sigma_i^2(z_i)}} \exp \times \left[-\frac{(\tau_{\rm th}^{\rm eff}(\Omega_b, a_0, a_1, a_2, \sigma_{\rm int} \mid z_i) - \tau_{\rm ob}^{\rm eff}(z_i))^2}{2\sigma_i^2(z_i)} \right] \quad (9)$$

$\tau_{\rm th}^{\rm eff}$ is the predicted value of effective optical depth, $\tau_{\rm ob}^{\rm eff}$ is the corresponding observational data. In this paper, we set $\Omega_m = 0.315$, and $h = 0.701 \pm 0.101$ (Planck Collaboration et al. 2020). a_0, a_1, a_2 are three parameters related to Γ_{-12}. Where $\sigma_i(z_i)^2 = \sigma_\tau^2(z_i) + \sigma_{\rm int}^2$, $\sigma_\tau^2(z_i)$ is the error in effective optical depth data. $\sigma_{\rm int}$ is the global intrinsic dispersion.

To calculate the posterior distribution of the model parameters, we employed the Affine Invariant Markov Chain Monte Carlo (MCMC) ensemble sampler, emcee (Foreman-Mackey et al. 2013), implemented in Python. This method allowed us to survey the posterior distribution in the parameter space and maximize the likelihood function. The resulting contour plots were generated using the corner module (Foreman-Mackey 2016).

4. Discussion and Conclusion

For the first data set from Fan et al. (2006), the constraining results are shown in Figure 3. Since the data is concentrated in the high-redshift range, the parameters a_0 and a_1 corresponding to the low redshift part of the curve

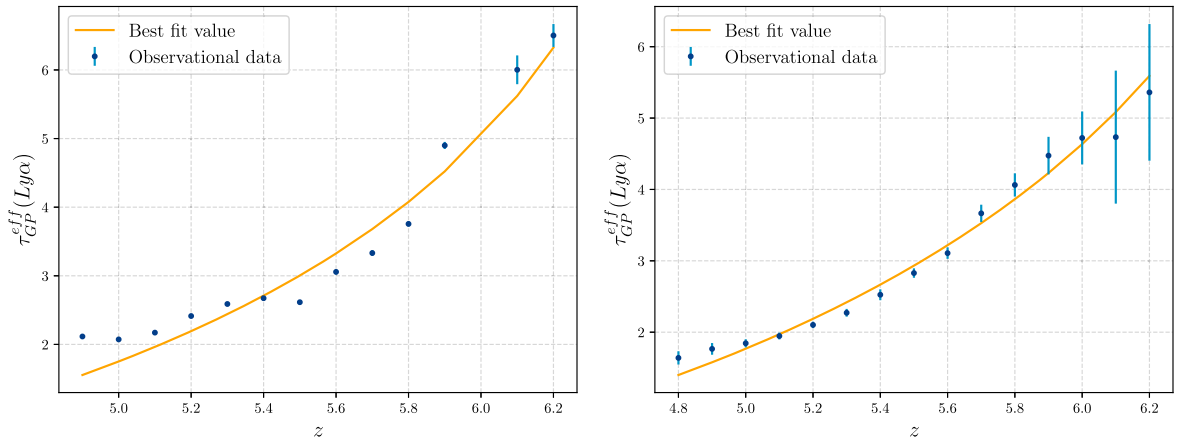

(a) Data from Fan et al. (2006) (b) Data from Bosman et al. (2022)

Figure 5. Theoretical values and observed effective optical depths for Lyα data. The theoretical values are represented by yellow triangles, while the observed values are shown as blue points with error bars. We can see that the results from the two data sets fit well and are consistent.

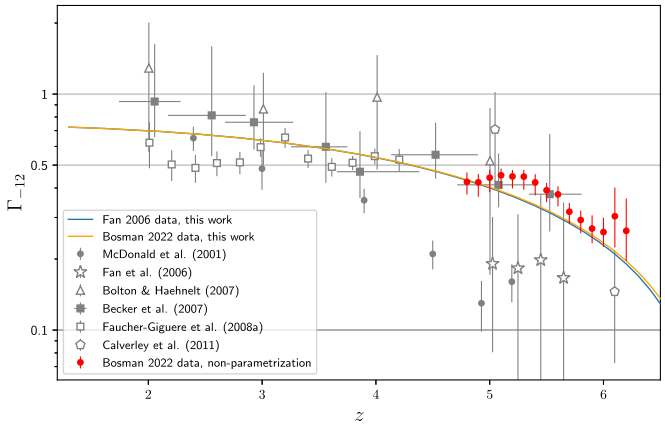

Figure 6. The photoionization rate has been reconstructed along with the 1σ confidence interval. The orange curve represents the results from Fan et al. (2006), while the blue curve corresponds to the findings of Bosman et al. (2022). Data with error bars represent previous measurements of Γ_{-12}. Filled circles denote empirical measurements from the Lyα forest effective opacity by McDonald & Miralda-Escudé (2001). Stars are from Fan et al. (2006). Triangles are from Bolton & Haehnelt (2007). Filled squares are from Becker et al. (2007). Squares are from Faucher-Giguere et al. (2008). Pentagons represent measurements using the quasar proximity effect by Calverley et al. (2011). Note that all those previous measurements require an assumption on cosmological parameters, such as h, Ω_m, and Ω_b. Although such a comparison may not be particularly meaningful, intuitively, our results are consistent with previous measurements that depended on cosmological parameters. The red dot with the error bar represents the non-parametric form of Γ_{-12}, which is also consistent with previous work.

cannot provide a strong constraint. Nevertheless, we have successfully constrained the baryon density, Ω_b, with a best-fit value of $0.043^{+0.005}_{-0.006}$. This finding supports a universe that is in agreement with the results from Planck Collaboration et al. (2020). The 1σ confidence region is narrow, indicating high precision in our test results. Additionally, the left panel of Figure 5 shows the Lyα data and its theoretical values with the constrained parameters, while Figure 6 displays the reconstructed shape of $\Gamma_{-12}(z)$. We can observe that the photoionization rate decreases with redshift, indicating the presence of abundant neutral hydrogen during the early stages of the universe.

For the second data set from Bosman et al. (2022), the constraining results are shown in Figure 4. We obtain a slightly larger value of $\Omega_b = 0.045^{+0.004}_{-0.006}$ compared to that of Fan et al. (2006). Those results for Ω_b are in good agreement with Planck Collaboration et al. (2020) within the 1σ confidence region. The right panel of Figure 5 shows the fitting results.

Figure 6 shows the reconstructed ionization rate. It is clear that the results from the two data sets are similar at high redshift but exhibit a larger dispersion at low redshift. This is expected as we are using high-redshift data. We also tested the robustness of the parameterization of Γ_{-12} using a 4-parameter Bézier polynomial and a 5-parameter Bézier polynomial. The test results are shown in Figures 7 and 8, respectively. Compared to the 3-parameter case, the 4- and 5-parameter Bézier polynomials yield larger values of $\Omega_b = 0.048^{+0.004}_{-0.007}$ and $\Omega_b = 0.049^{+0.004}_{-0.006}$, respectively, which, however, remain consistent with the Planck results within 1σ.

A higher baryon fraction would lead to an increased number of electrons available for scattering photons, thereby augmenting the electron scattering optical depth. Furthermore, a greater baryon fraction implies a larger pool of baryons ready for star and galaxy formation. This could potentially stimulate galaxy

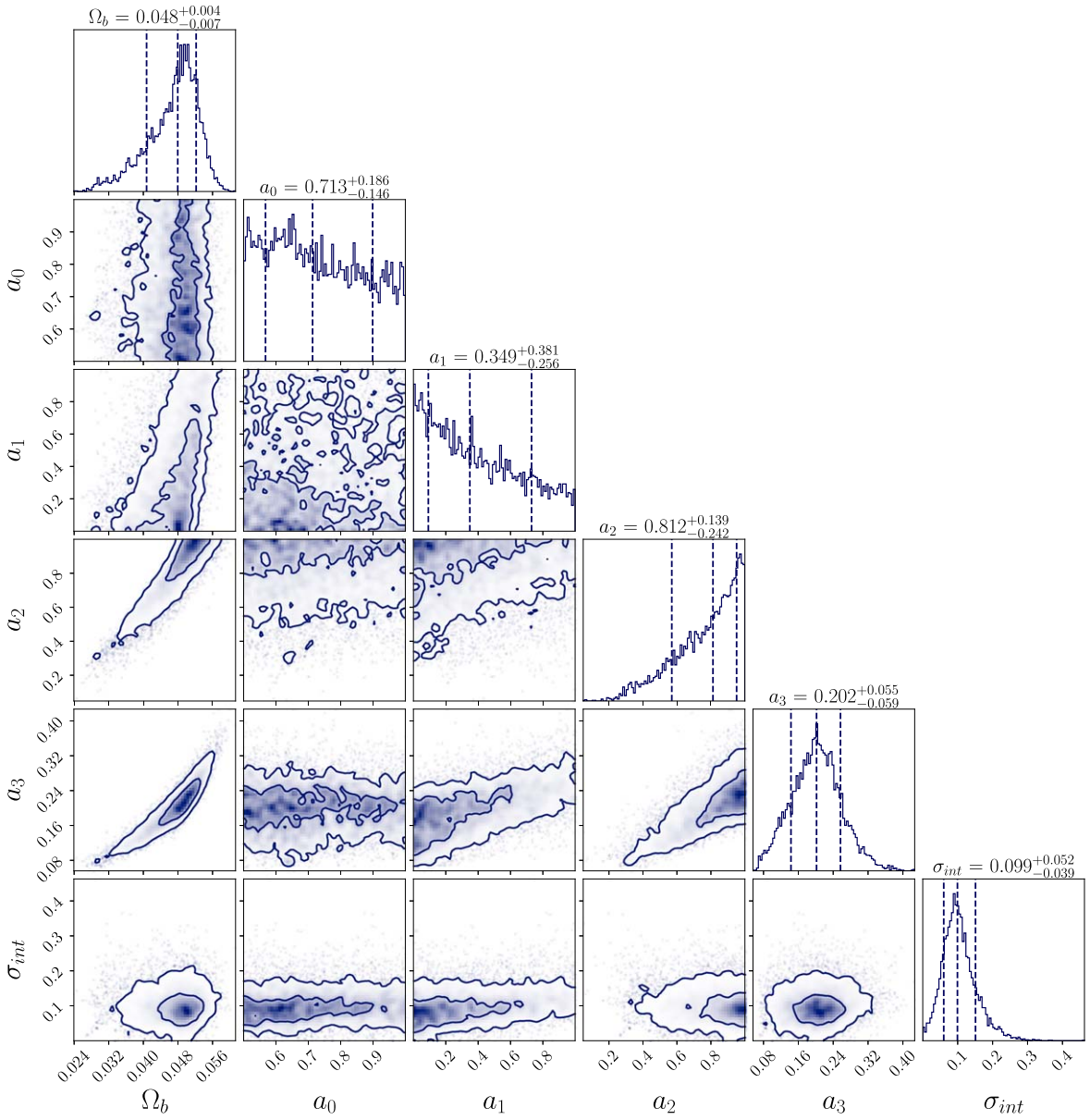

Figure 7. The 1D and 2D contours represent the 1σ and 2σ confidence regions for the Lyα data from Bosman et al. (2022), using a Bézier polynomial with four parameters. It can be seen that the baryon density obtained with four parameters is slightly higher than that with three parameters, but it is consistent with the three-parameter results within the 1σ confidence interval.

formation and evolution at higher redshifts. The elevated baryon fraction can also influence feedback processes within galaxies. Feedback mechanisms, such as supernovae explosions and active galactic nuclei, control the growth of galaxies by infusing energy and momentum into the surrounding gas. With a higher baryon fraction, these feedback processes could become more efficient, potentially impacting the gas dynamics, star formation rates, and overall galaxy properties at higher redshifts. This could provide a more direct explanation for the recent observations made by the James Webb Space Telescope (JWST) of more massive galaxies at these redshifts than previously anticipated (Labbé et al. 2023). Another possible reason for the larger Ω_b value might be the relatively limited amount of data. However, this result still includes Planck's results within the 1σ region. Therefore, we must admit that the slight increase in Ω_b is not sufficient to explain the abundance of bright galaxies at an early age. The parameterization form has a mild effect on the final results.

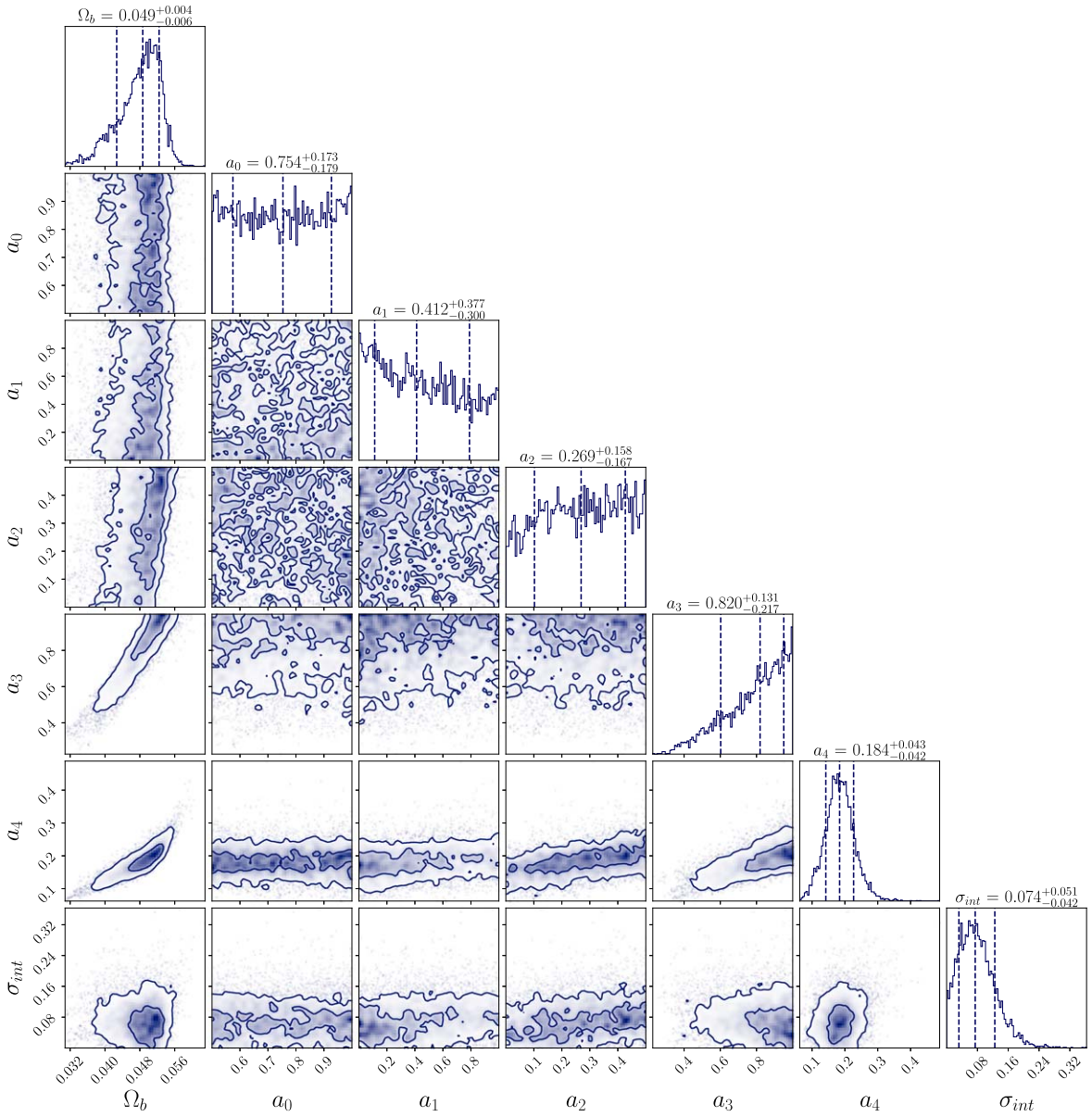

Figure 8. The 1D and 2D contours represent the 1σ and 2σ confidence regions for the Lyα data from Bosman et al. (2022), using a Bézier polynomial with five parameters. Similar to the four-parameter case, the constraint results for the function parameters are consistent with the three-parameter results within the 1σ confidence interval.

We believe that the constraining power on Ω_b originates from redshift dependence. Equation (2) demonstrates the degeneracy between Γ_{-12} and Ω_b at a specific redshift. However, by combining data from different redshifts, we could break this degeneracy and place a strong constraint on Ω_b. In such a case, Ω_b would affect the amplitude of the $\tau_{\rm eff}$ curve, while Γ_{-12} would influence both the amplitude and shape of the curve. Therefore, we test the non-parametric form of $\Gamma_{-12}(z)$. We use 15 parameters g_i for i ranging from 0 to 14, each representing Γ_{-12} at a specific redshift in the data. Because the data lie in the high-redshift range, we assume these parameters have a flat prior of $(0 \sim 0.5)$. The test results are shown in Figure 6, and the corner plot for g_i is displayed in Figure 9. From the plots, we can see that the baryon density parameter is well constrained: $\Omega_b = 0.048^{+0.001}_{-0.003}$. The constraining power remains strong even with the non-parametric form of Γ_{-12}.

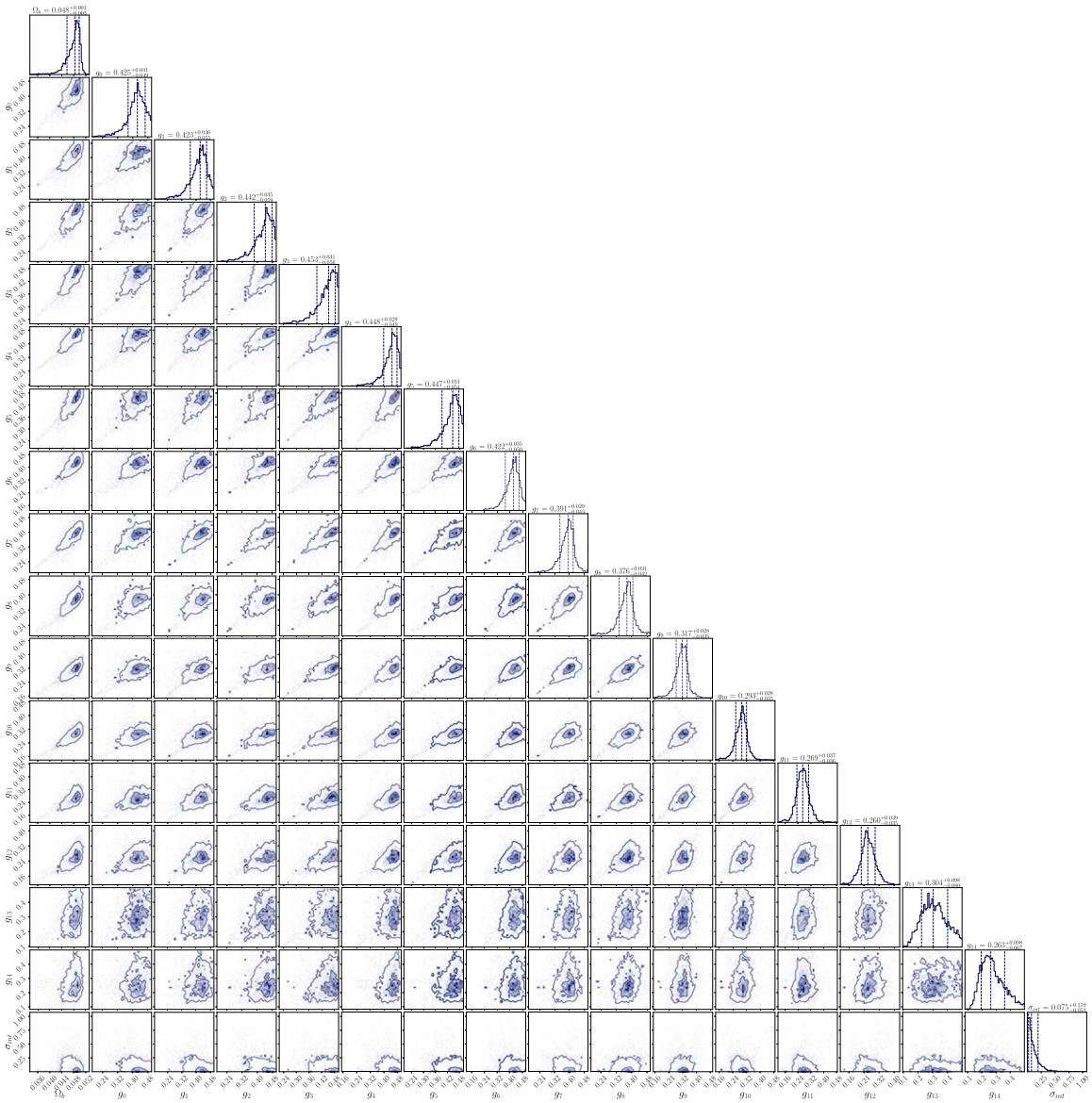

Figure 9. The 1D and 2D contours represent the 1σ and 2σ confidence regions for the Lyα data from Bosman et al. (2022), using 15 Γ_{-12} parameters at each redshift. It is clear that the constraining power remains strong, allowing Ω_b to be determined with small uncertainties.

Another important factor that could dramatically influence the results is the distribution function of the intergalactic medium's density, which is shaped by Equation (5). We examined the influence of the four parameters on $\tau_{\rm eff}$ and displayed the results in Figure 10. It is evident that these variations in the four parameters significantly affect $\tau_{\rm eff}$. Therefore, the robustness of our results partially depends on the accurate and comprehensive understanding of the IGM properties, especially the density distribution of the IGM.

In conclusion, this study represents the first effort to use two sets of effective optical depth data, obtained from high-redshift quasars, to constrain the cosmological parameter Ω_b. We found that incorporating photoionization rate data is not crucial, as the parameterization of Γ_{-12} proves effective when ample data are available. Despite the limited data set, our analysis yielded highly precise results with minimal uncertainties, showing good consistency with Planck Collaboration et al. (2020). Our work is valid for high-redshift $z \gtrsim 4.5$. A high precision of thermal history and the correct shape of the density distribution are crucial for constraining Ω_b. Future research will aim to refine the constraints on Ω_b by combining these findings with data from low-redshift celestial objects such as supernovae, the Hubble parameter,

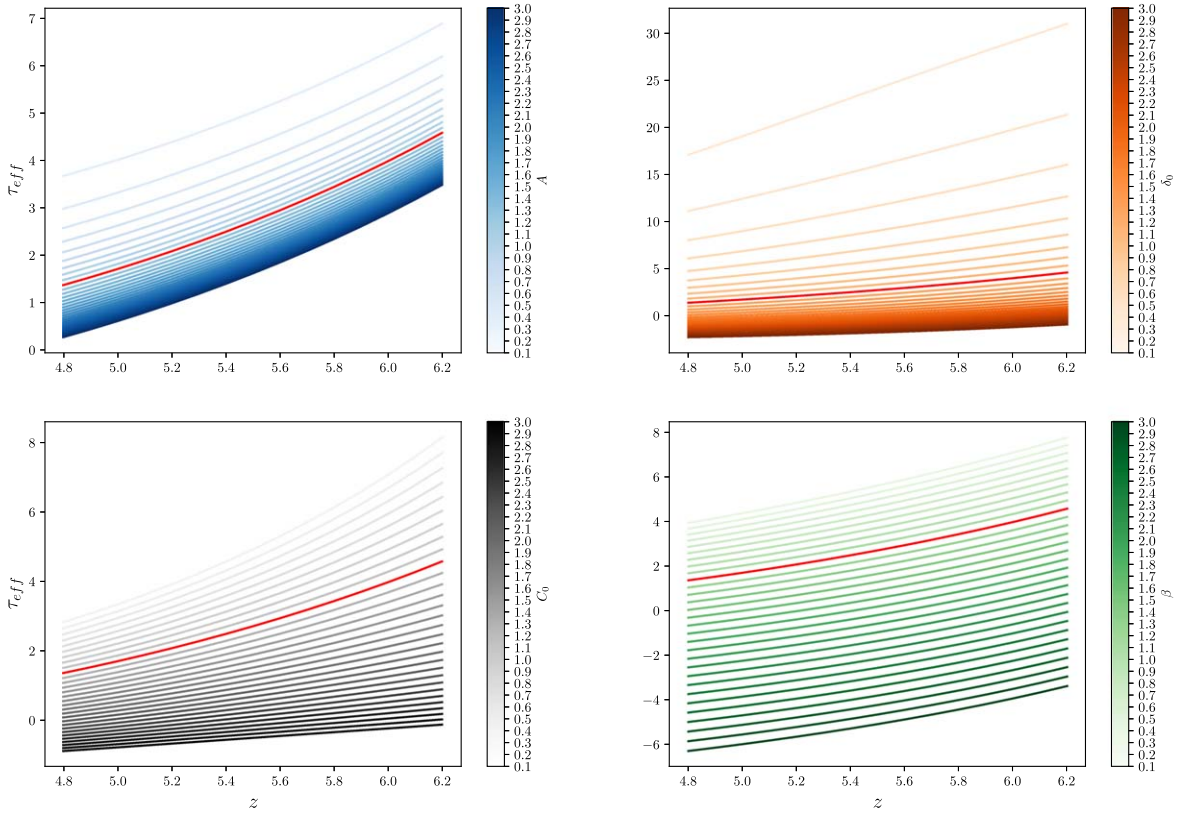

Figure 10. The influence of density PDF parameters A, δ_0, C_0, and β on $\tau_{\rm eff}$ is substantial. Each parameter was adjusted by a factor ranging from 0.1 to 3. It is evident that those parameters will significantly affect $\tau_{\rm eff}$. Therefore, our result depends on the robustness of those parameters.

and BAO. This integrated approach promises to further enhance our understanding of Ω_b.

Acknowledgments

We are grateful for the insightful and useful comments of the referee that greatly helped us improve our manuscript. T.J.Z. (张同杰) dedicates this paper to the memory of his mother, Yu-Zhen Han (韩玉珍), who passed away 4 yr ago (2020 August 26). This work was supported by the National SKA Program of China (2022SKA0110202) and China Manned Space Program through its Space Application System.

References

Abel, T., Anninos, P., Zhang, Y., & Norman, M. L. 1997, NewA, 2, 181
Amati, L., D'Agostino, R., Luongo, O., Muccino, M., & Tantalo, M. 2019, MNRAS, 486, L46
Becker, G. D., Bolton, J. S., Madau, P., et al. 2015, MNRAS, 447, 3402
Becker, G. D., Rauch, M., & Sargent, W. L. W. 2007, ApJ, 662, 72
Becker, R. H., Fan, X., White, R. L., et al. 2001, AJ, 122, 2850
Bolton, J. S., & Haehnelt, M. G. 2007, MNRAS, 382, 325
Bosman, S. E. I., Davies, F. B., Becker, G. D., et al. 2022, MNRAS, 514, 55
Calverley, A. P., Becker, G. D., Haehnelt, M. G., & Bolton, J. S. 2011, MNRAS, 412, 2543
Djorgovski, S., Castro, S., Stern, D., & Mahabal, A. 2001, ApJL, 560, L5
Fan, X., Narayanan, V. K., Lupton, R. H., et al. 2001, AJ, 122, 2833
Fan, X., Narayanan, V. K., Strauss, M. A., et al. 2002, AJ, 123, 1247
Fan, X., Strauss, M. A., Becker, R. H., et al. 2006, AJ, 132, 117
Faucher-Giguere, C.-A., Lidz, A., Hernquist, L., & Zaldarriaga, M. 2008, ApJL, 682, L9
Foreman-Mackey, D. 2016, JOSS, 1, 24
Foreman-Mackey, D., Hogg, D. W., Lang, D., & Goodman, J. 2013, PASP, 125, 306
Gunn, J. E., & Peterson, B. A. 1965, AJ, 142, 1633
Hernquist, L., Katz, N., Weinberg, D. H., & Miralda-Escude, J. 1996, ApJL, 457, L51
Holt, S. S., & Smith, E. P. 1999, in 9th Annual Astrophysics Conf. (New York, NY: AIP)
Hui, L., & Gnedin, N. Y. 1997, MNRAS, 292, 27
Kulkarni, G., Keating, L. C., & Haehnelt, M. G. 2019, MNRAS, 485, L24
Labbé, I., van Dokkum, P., Nelson, E., et al. 2023, Natur, 616, 266
McDonald, P., & Miralda-Escudé, J. 2001, ApJL, 549, L11
McQuinn, M., & Upton Sanderbeck, P. R. 2015, MNRAS, 456, 47
Miralda-Escudé, J., Haehnelt, M., & Rees, M. J. 2000, ApJ, 530, 1
Pentericci, L., Fan, X., Rix, H.-W., et al. 2002, AJ, 123, 2151
Planck Collaboration, Aghanim, N., Akrami, Y., et al. 2020, A&A, 641, 67
Rauch, M., Miralda-Escud, J., Sargent, W. L. W., et al. 1997, ApJ, 489, 7